The solar magnetic field and the solar wind: Existence of preferred longitudes

M. Neugebauer, E. J. Smith, A. Ruzmaikin, J. Feynman, and A.H. Vaughan

Jet Propulsion Laboratory, California Institute of Technology, Pasadena

Abstract

Direct measurements of the solar wind and the interplanetary magnetic field acquired over more than three solar cycles both near Earth and in interplanetary space are used to search for signatures of a persistent dependence of solar wind properties on solar longitude. Two methods of analysis are used. One is based on both interplanetary and near-Earth data mapped to the Sun. The other is based on power spectra of near-Earth or near-Venus data. The two methods give the same result. Preferred-longitude effects are found for a synodic solar rotation period of 27.03 ± 0.02 days. Such high precision is attained by using several hundred thousand hourly averages of the solar wind speed and magnetic field. The 27.03-day periodicity is dominant only over long periods of time; other periodicities are often more prominent for shorter intervals such as a single solar cycle or less. The 27.03-day signal is stronger and more consistent in the magnetic field than in the solar wind speed and is stronger at for intervals of high and declining solar activity than for intervals of low or rising activity. On average, solar magnetic field lines in the ecliptic plane point outward on one side of the Sun and inward on the other, reversing direction approximately every 11 years while maintaining the same phase. The data are consistent with a model in which the solar magnetic dipole returns to the same longitude after each reversal.

Introduction

A considerable body of evidence that recurrent solar activity is associated with specific solar longitudes has accumulated over the years. *Trotter and Billings* [1962] discerned a longitudinal persistence of solar active regions over one solar cycle, but not from one cycle to the next. *Bumba and Howard* [1969] demonstrated rigid rotation of low-latitude (±20°) patterns in the solar magnetic field which persisted for several months. *Svalgaard and Wilcox* [1975] showed that the longitudinal structure of the polarity of the interplanetary magnetic field persisted for five solar cycles with a period of 27 days. On an even longer time scale, *Bogart* [1982] found a persistence of 27-day modulations of daily sunspot numbers over a period of 128 years, consistent with long-lived active longitudes. This periodicity was found to be strong in some solar cycles and weak in others, however, and no attempt was made to compare the phases of sunspot variations in cycles for which the periodicity was present. As for the solar wind plasma, *Gosling et al.* [1977] found evidence for a longitudinal dependence of solar wind speed for the 11.5-year interval July, 1964 to December, 1975, and a study by *Mursula and Zieger* [1996] covering three solar cycles revealed a 13.5-day periodicity of the solar wind speed whose amplitude and phase varies with time. In this paper we address the question of whether, despite the highly variable character of the Sun and the many manifestations of its activity, are there preferred longitudes that persist from one sunspot cycle to another?

The existence, or absence, of preferred solar longitudes over long periods of time would have implications for our understanding of natural dynamos and of solar and stellar activity. In the case of the Earth's magnetic field, the non-axisymmetric component of the secular variation can be resolved into two parts, one of which drifts in longitude with time and another which does not. There are also hints of preferred longitudes in Sun-like stars. Observations of stellar magnetic activity via monitoring of calcium II H and K emissions provides evidence that some stars have preferred longitudes that persist over several activity cycles [*Vaughan et al.*, 1981;*Vaughan*, 1984]; in some cases the preferred longitude appears to shift by ~180° (A.H. Vaughan and S.L. Baliunas, unpublished paper presented at IAU Colloquium No. 141, Beijing, China, September, 1992).

The properties of the solar wind and the interplanetary magnetic field (IMF) have now been measured, with some interruptions, for 37 years. Motivated by earlier reports suggesting the reality of preferred solar longitudes and by current work on stellar activity, we here use a very large data base to extend previous analyses of time variations of the solar wind to cover a period of more than three solar cycles of direct measurements.

Data Sources

The study is based on hourly averages of the solar wind speed and the IMF observed near Earth and in interplanetary space over the period 1962 to

1998. The data were acquired from the National Space Science Data Center (NSSDC). Except for the Mariner 2 and Pioneer 6 and 7 data sets, the data are available in the COHO (Coordinated Heliospheric Observations) data base. We converted the Mariner 2 and Pioneer 6 and 7 data supplied by NSSDC to the COHO format and can provide the converted data to other researchers on request. Magnetic field data from Mariner 2 are not used because of the large uncertainty in the spacecraft field.

The following parameters are used from this COHO-formatted data base: t_{obs} is the time of observation in integer hours since the start of 1962; λ_{obs} is the spacecraft longitude in heliographic inertial (HGI) coordinates, which are Sun centered and inertially fixed with respect to an axis along the intersection of the ecliptic and solar equatorial planes; R_{obs} is heliocentric distance, in AU; V is the observed hourly-averaged solar wind speed in km/s; and B_r is the radial component of the magnetic field in nT, normalized to 1 AU by multiplying the measured value by R_{obs}^2.

The sources of data are listed in Table 1, together with the years of observation, the number of hours of speed data, and the number of hours with both speed and magnetic field data. Inaccuracies in mapping the solar wind back to the Sun are limited by using only data acquired at solar distances less than 3 AU. For Ulysses, only the data acquired during the in-ecliptic phase of the mission are used. The study is based on 334,763 hours of speed data and 246,834 hours of field data. Note that using interplanetary data in

addition to the near-Earth OMNI data doubles the number of hourly averages available for analysis, thus providing precision not previously attained.

Data Mapped Back to the Sun

For each hour of data, the constant-speed, radial-flow approximation is used to map the solar wind from the spacecraft to the Sun and to determine the time the plasma left the Sun and the longitude of the source region. The time t_s when the solar wind left the Sun is given (in hours since the start of 1962) by

$$t_s = t_{obs} - 41556\, R_{obs}/V \qquad (1)$$

Because the flow is assumed to be radially outward from the Sun in an inertial frame of reference, the longitude λ of the solar source, in HGI coordinates, is the same as the longitude at which the data are obtained:

$$\lambda \text{ (at time } t_s) = \lambda_{obs} \text{ (at time } t_{obs}) \qquad (2)$$

If λ_e is the HGI longitude of Earth at time t_s, then the difference in longitude between the solar wind source and the sub-Earth point is

$$\Delta\lambda = \lambda - \lambda_e \tag{3}$$

For this study we are interested in the solar longitude ϕ rather than in the inertial longitude λ. Solar longitude depends on two parameters: the solar rotation period P and a definition of the zero of longitude. The rotation period is determined by the data, as explained in the next paragraph. Zero longitude is arbitrarily defined to be the sub-Earth solar meridian at 0000 UT on Jan 1, 1962. For P = 27 days, our solar longitude is related to the Bartels rotation used in the study of geomagnetic activity; for an average travel time of the solar wind from the Sun to the Earth of 4 days, each Bartels rotation would start at 253° in our longitude system.

The steps in the analysis are as follows: (1) A synodic solar rotation period P (e.g., P = 27.0 days) is assumed. (2) The solar longitude ϕ of a solar-wind source region is then calculated from t_s and $\Delta\lambda$ as follows:

$$\tau = (t_s - t_o)/(24\,P) \tag{4}$$

where τ is the number of rotations since time t_o = 0000 UT on Jan 1, 1962. The solar longitude of Earth, in degrees, is

$$\phi_e = 360° \times [\text{the fractional part of } \tau \; = \text{mod}(\tau, 1.0)] \tag{5}$$

and the solar longitude of the solar wind source region is then

$$\phi = \phi_e - \Delta\lambda \tag{6}$$

The integer part of τ provides a rotation counter. (3) The solar wind speed V and the normalized radial component of the field B_r are then binned according to the values of τ and ϕ. The τ bins are one solar rotation in duration, and the ϕ bins are 10° wide. The longitudinal resolution of 10° is chosen to match the approximate accuracy of the mapping procedure [*Nolte and Roelof*, 1973]. (4) After all the data from all the spacecraft are mapped back, average values of V and B_r are calculated for each bin to obtain two matrices, each with 36 columns (longitudes) and ~500 rows (solar rotations). The precise number of rows depends on the rotation period. (5) Each column of the speed matrix is averaged to yield time-averaged speed versus longitude. (6) Steps 1 through 5 are repeated for a number of different rotation periods.

Time-averaged longitudinal speed profiles are shown for ten different rotation periods between 24 and 33 days in Figure 1. The longitudinal modulation of the speed is flat, within the probable-error bars, for periods of 24, 25, 32, and 33 days. The greatest longitudinal modulations appear at 27 and 28 days. Figure 2 shows the results for trial periods separated by 0.01 days, where the abscissa is the assumed period and the ordinate is the speed range,

which is the amplitude (peak to minimum) of the speed variation with longitude. The largest amplitude variation occurs at a period slightly greater than 27 days; for periods between 27.01 and 27.05 days the speed range exceeds the range of all the other peaks. This result agrees with the rotation period of 27.025 days for the 11-year interval 1964-1975 studied by *Gosling et al.* [1977]. The second highest peak occurs at P = 28.00 days.

Analysis of the mapped-back values of B_r is complicated by the polarity reversal of the solar magnetic field approximately every 11 years; any longitudinal variation of B_r would be washed out in grand averages over the entire period of analysis as was done for the speed in Figures 1 and 2. A contour plot (not shown) of the longitude-time matrix for the field data for P = 27.03 days suggests that the reversal of the in-ecliptic IMF occurs neither near solar maximum, when the solar surface field reverses, nor near solar minimum, but during times of increasing solar activity.

A more quantitative estimate of the time of reversal of the IMF is obtained by first smoothing the data in the longitude-time B_r matrix by taking 5-point running averages in each dimension, and then fitting the value of B_r in every second longitude and every second time bin to a function of the form

$$B_r = B_{ro} \sin(\phi - \phi_o) \sin(\theta - \theta_o) \tag{7}$$

$$\theta = 360^\circ \tau/292 \tag{8}$$

where B_r and ϕ are values from the smoothed matrix and the factor 292 in (8) is the number of 27.03-day rotations in a 21.6-year solar magnetic cycle (an average cycle length for the years 1954-1996). The unknowns B_{ro}, ϕ_o, and θ_o are solved for by least squares. The result is B_{ro} = 1.35 nT, ϕ_o = 328°, and θ_o = 259°. This value of θ_o corresponds to reversals of the IMF at years 1966.74 + 10.8N, where N = 0, 1, 2, 3. We therefore define four solar cycles, called Cycle A through Cycle D as summarized in Table 2, and change the sign of B_r for Cycles B and D. In all further calculations involving the magnetic field, we use the parameter $B_r(-1)^N$; the sign change is equivalent to a 180° phase shift of B_r in alternate cycles.

The relation of our Cycles A-D to the sunspot cycle is shown in Figure 3. The sunspot data are monthly averages obtained from http://ftp.ngdc.noaa.gov/stp/solar_data/. The sign reversal occurs during the rising phase of the solar activity cycle slightly before solar maximum. This is, of course, only a simple approximation to the complex reversals of the solar magnetic field. It is perhaps interesting to note that this change of sign of the in-ecliptic magnetic field occurs more than a year before the reversals of the solar polar magnetic fields.

With this change of sign in alternate cycles, the field data are then processed in the same way as the speed data, resulting in Figure 4. The highest peak in Figure 4 extends from 27.01 to 27.06 days, in agreement with

the speed data. For the field data, the second highest peak is at 28.27 days, which is different from the 28.00-day second peak in the speed data.

An important question is whether the longitudinal variation associated with a period of 27.03 days persists over the entire period or whether the amplitudes of the variations in specific cycles, e.g., 1964-1975, are so large that they dominate the variation for the entire period. This question is addressed by analyzing the data for each cycle separately. Figure 5 shows time-averaged V and $B_r\,(-1)^N$ versus longitude for a rotation period of 27.03 days for Cycles A through D. Although there are speed maxima at ~60° longitude in each cycle, the speed profiles exhibit great variation from one cycle to the next, with Cycles B having two peaks, Cycle C having very little modulation, and Cycle D being intermediate between Cycles B and C. The field data do exhibit cycle-to-cycle regularity, however, with maxima at ~30° and minima between 200° and 250° in each cycle.

The plots for Cycle B are a good illustration of the Earth encountering two high-speed streams with opposite magnetic polarities per solar rotation. Such a topology is often encountered during periods of declining solar activity when the Sun has large polar coronal holes which reach down to low latitudes due to the tilt of the solar magnetic dipole (e.g., [*Hundhausen*, 1977]). The high-speed wind from the northern polar coronal hole has the opposite magnetic polarity than the high-speed wind from the southern polar coronal hole which is observed half a rotation later.

The range-versus-period plots similar to Figures 2 and 3 are shown for each cycle in Figure 6. For reference, the dashed lines indicate a period of 27.03 days. The speed data for Cycle C show little modulation at any period, whereas there is a peak near 27.03 days for Cycles A, B, and D, although it is not always the largest peak. For the field data, there is a peak near 27.03 days for Cycles B, C, and D, but a minimum at that period for Cycle A for which there is very little field data.

Analysis of time-series data

The speed and field variations can also be analyzed as simple time series rather than as longitude-time matrices. It is not, however, possible to combine the interplanetary data with the near-Earth data for this type of analysis because corotating the interplanetary data to Earth requires knowledge of the solar rotation period, which is the unknown parameter we are trying to find. We are thus limited to using the OMNI data set for which the statistics of data coverage are given in Table 3. Because we are interested only in periodicities in the neighborhood of 27 days, we decrease the computational time and increase the per-cent data coverage by forming 12-hour averages of V and B_r. The data coverage is still rather poor, with 35.6% and 34.9% gaps in the speed and field data, respectively. Because of the of the large fraction of missing data, we use the Lomb-Scargle periodogram method

[*Press et al.*, 1992] of computing spectral power as a function of frequency or period.

Figure 7 shows the periodograms of V and $B_r(-1)^N$ from the OMNI data. Both panels show power enhancements near periods of 13.5 days, 27 days, and 1 year. *Fenimore et al.* [1978] previously showed that there is frequently more power in the solar wind speed spectrum at 13.5 days than at 27 days. *Mursula and Zieger* [1996] studied the 13.5-day periodicity of the solar wind and interplanetary magnetic field in greater detail and found that it is most prominent during solar-cycle phases when the Earth encounters two high-speed streams per solar rotation. The peaks near one year are probably a latitudinal dependence of V and B_r caused by the annual variation of the heliographic latitude of the Earth. The highest peak in the speed periodogram falls at 9.38 years, which is near, but somewhat less than the 10.8-year periodicity in the sunspot cycle. Changing the sign of B_r in alternate cycles leads to the disappearance of a peak at ~22 years for that parameter.

The peaks near 27 days are shown at higher resolution in Figure 8. Both V and $B_r(-1)^N$ have strong maxima in their periodograms near 27.03 days, which is indicated by the vertical line, thus confirming the results found in the previous section (Figures 2 and 4).

Press et al. [1992] provide an estimate of the probability that a periodogram peak of height z is the result of random noise rather than a true periodic signal. For the V and $B_r(-1)^N$ periodogram peak heights shown in

Figure 8, their algorithm gives formal null hypothesis probabilities of 10^{-17} and 10^{-161}, respectively. *Hernandez* [1999] argues that the null hypothesis probability should be calculated from the half-height $z/2$, rather than from z, which would yield null probabilities of $10^{-6.5}$ and 10^{-79}, which are still remarkably small numbers. The periodogram method can give spurious peaks when the data stream contains periodic data gaps, and there are also questions concerning the number of independent frequencies or degrees of freedom that enter the calculation of probabilities [*Horne and Baliunas*, 1986; *Hernandez*, 1999]. We therefore computed periodograms for a series of Gaussian random numbers, with variances equal to the observed variances of V and $B_r(-1)^N$, sampled at the same unevenly-spaced times as the observations. The resulting periodograms are also plotted in Figure 8 as lines without data points on them. There is very little power in the periodograms derived from the random data. The 27.03-day peak in the V periodogram in Figure 8 is 5.6 times higher than the highest peak in the random-V periodogram, indicating at least a 5-σ result. A similar analysis for the field data shows that the 27.03 day periodicity in $B_r(-1)^N$ is significant at the 29-σ level or more. Note that neither random periodogram has a peak at 27.03 days. We conclude that false peaks due to periodic gaps are not a concern.

Of the spacecraft well removed from Earth and not contributing to the OMNI data set, only Pioneer Venus Orbiter (PVO) provides a good opportunity for time-series analysis. The PVO magnetometer data set runs

nearly ten years from December, 1978 to August, 1988, and thus nearly coincides with our Cycle C. The fractional coverage of 12-hour averages of the magnetic field observed at PVO is 0.713. A periodogram is calculated as a function of the period P_v observed at Venus and the result is then transformed to the period P_e which would be observed if the spacecraft were at Earth. It can be shown that

$$1/P_v + 1/Y_v = 1/P_e + 1/Y_e \tag{9}$$

where Y_v = 224.701 days and Y_e = 365.256 days are the lengths of the Venusian and terrestrial years, respectively. The resulting periodogram of $B_r(-1)^N$ observed at Venus versus P_e is shown in Figure 9 together with the nearly simultaneous periodogram obtained from the OMNI data for Cycle C. The two periodograms have peaks at nearly the same values of P_e, with the PVO data have a higher (more significant) peak near 27 days than the OMNI data. This peak is centered at a period slightly less than 27 days, consistent with the Cycle C data shown on the right side of Figure 6.

Dependence on solar-cycle phase

The analyses presented in the two previous sections are based on averages either over the entire duration of direct observations of the solar wind or over 10.8-year solar cycles. A remaining question is whether the presence of the periodicity of 27.03 days depends on the phase of the solar cycle. We choose a dividing line between sunspot maximum and sunspot

minimum at a sunspot number of 70, indicated by the horizontal line in Figure 3. A period of maximum (minimum) activity is defined to start the first time the sunspot number exceeds (drops below) a value of 70. The lowest and highest monthly means for each cycle shown in Figure 3 are used to define the boundaries of intervals of rising and declining activity. Figure 10 shows periodograms of $B_r(-1)^N$ calculated separately for intervals of sunspot maximum and maximum and rising and declining activity. The highest peak is that at 27.03 days for $B_r(-1)^N$ at solar maximumThere is also a signigicant 27.03-day peak for periods of declining activity, but not at solar minimum or during the rise to maximum. Similar periodograms for the solar wind speed did not show a dominant 27.03-day peak for any of the individual activity phases.

Discussion and conclusions

The two methods of analysis, one based on both interplanetary and near-Earth data mapped to the Sun and the other based on power spectra of near-Earth or near-Venus data, give the same results. When the data sets are taken as a whole, there is a statistically significant periodicity at 27.03 ± 0.02 days. The uncertainty of ±0.02 days corresponds to the widths of the 27.03-day peaks in Figures 2 and 4. The full width at half maximum of the $B_r(-1)^N$ periodogram in Figure 8 is ±0.03 days. The precision is limited by the amount of data used, and less data was used in the periodogram analysis than in the

method based on the amplitude of speed and field variations mapped back to the Sun.

Most of the emphasis, especially in the periodogram analysis, has been focussed on determination of the rotation period. But the uncertainty in the rotation rate can be use to place limits on the longitudinal drift of features in the solar wind speed and magnetic field. The change in solar longitude $\Delta\phi$ in a time span Δt is given by

$$\Delta\phi = 360° \, \Delta t \, / P \tag{10}$$

Differentiation of Equation (10) yields a relation between the uncertainty in longitude $\delta(\Delta\phi)$ and the uncertainty δP in the period

$$\delta(\Delta\phi) = 360° \frac{\Delta t}{P^2} \delta P \tag{11}$$

According to Equation (11), for $\delta P = \pm 0.02$ days, a lower limit to the phase coherence time, defined as the time for $\Delta\phi$ to change by $\pm 90°$, is 25 years.

Figures 5, 7, and 8 demonstrate that the 27.03-day periodicity and the preferred longitude effect are much more pronounced in the magnetic field than in the solar wind speed. This result is consistent with the contemporary view that the solar magnetic field configuration controls the acceleration of the solar wind. In this respect, the magnetic field is a more fundamental

parameter than is the speed. Furthermore, the solar wind speed is modified by the interaction of fast and slow streams in interplanetary space while the polarity of the interplanetary field remains unaffected.

It cannot be overemphasized that the 27.03-day periodicity can be discerned only over long periods of time. It is less apparent when the data are analyzed a magnetic cycle at a time, and it is stronger for maximum and declining solar activity maximum than for intervals of minimum and rising activity. In most of the subsets of the data base, there are additional periodicities, some of which are stronger than that at 27.03 days.

Disk integrated solar calcium emission shows similar properties (A. Ruzmaikin and J. Feynman, paper in preparation). This behavior is also similar to that seen in stellar observations where an apparent rotational modulation of the calcium emission comes and goes, but when it is present, it usually (but not always) has the same phase (A.H. Vaughan and S.L. Baliunas, unpublished paper presented at IAU Colloquium No. 141, Beijing, China, September, 1992).

In Table 4, the rotation period found in this study is compared to rotation periods found from studies of other solar phenomena. Our results agree very closely with the periodicity of solar wind speed observed by *Gosling et al.* [1977] in 1964-1975 and with the stronger of two periodicities found by *Svalgaard and Wilcox* [1975] from their analysis of sector boundary crossings over four solar cycles. All measurements made in the solar wind are mutually consistent when one takes their differing precision into account.

The rotation periods of coronal holes and coronal magnetic fields appear to be slightly longer than that of the solar wind, but the time spans of the coronal measurements are not as long as the time spans of the solar wind measurements. The period of the photospheric magnetic field determined by *Snodgrass* [1983] equals 27.03 days at a latitude of ~9°. *Hoeksema and Scherrer* [1987] found a 27.0-day rotation rate for the dipole component of the photospheric magnetic field. Finally, the Michelson Doppler Imager on the SOHO mission has allowed the determination of the solar rotation rate as functions of latitude and distance from the center of the Sun. As shown in Table 4, the equatorial near-surface period is slightly longer than our 27.03 days, but decreases to something less than our value only 0.05 solar radii below the surface. A period of 27.03 days can be matched by some combination of increasing the latitude and increasing the depth.

Our result that the 27.03-day periodicity was much stronger at solar activity maximum than at minimum is perhaps surprising. We tend to think of high-speed recurrent solar wind streams as being a solar minimum phenomenon. Additionally, the geomagnetic *aa* index shows greater 27-day recurrence at solar minimum than at maximum [*Sargent*, 1985]. But the truth is that the equatorward extensions of the polar coronal holes which are the source of the recurrent high speed streams in the ecliptic occasionally shift their longitudes (e.g., [*Hundhausen*, 1977; *Balogh et al.*, 1993; *Macdowall et al.*, 1995; *Roelof et al.*, 1997]). Furthermore, the in-ecliptic fields are stronger at solar maximum than at minimum, while the passage of an increased number of

coronal mass ejections or magnetic clouds at solar maximum does not greatly disturb the underlying magnetic sector pattern [*Smith et al.*, 1986].

Our conclusion is that, on average, and especially at solar maximum, field lines point outward on one side of the Sun and inward on the other, reversing direction in alternate sunspot cycles. The preferred longitude found in this study may be caused by the non-axisymmetric component of the solar magnetic field (m = 1); over short periods of time this component cannot be discerned because of the temporary presence of higher moments. In an alternative view, the 27.03-day periodicity may be a state to which the Sun tends to relax, rather than being a permanent phenomenon. In analogy with the geomagnetic field, the solar magnetic pole returns to approximately the same longitude after each reversal. We look forward to seeing whether or not the preferred-longitude phenomena described in this paper persist over the next solar cycle or two.

Acknowledgments. We thank Joyce Wolf for converting the archived Mariner 2 and Pioneer 6 and 7 data to the COHO format and for teaching us about Gaussian random noise. This research was performed at the Jet Propulsion Laboratory of the California Institute of Technology under contract with the National Aeronautics and Space Administration.

References

Balogh, A., G. Erdös, R. J. Forsyth, and E. J. Smith, The evolution of the interplanetary sector structure in 1992, *Geophys. Res. Lett., 20*, 2331, 1993.

Bogart, R. S., Recurrence of solar activity: Evidence for active longitudes, *Solar Phys., 76*, 155, 1982.

Bumba, V., and R. Howard, Solar activity and recurrences in magnetic field distribution, *Solar Phys., 7*, 28, 1969.

Fenimore, E. E., J. R. Asbridge, S. J. Bame, W. C. Feldman, and J. T. Gosling, The power spectrum of the solar wind speed for periods greater than 10 days, *J. Geophys. Res., 83*, 4353, 1978.

Gosling, J. T., J. R. Asbridge, S. J. Bame, and W. C. Feldman, Preferred solar wind emitting longitudes on the Sun, *J. Geophys. Res., 82*, 2371, 1977.

Hernandez, G., Time series, periodograms, and significance, *J. Geophys. Res., 104*, 10355, 1999.

Hoeksema, J. T., and P. H. Scherrer, Rotation of the coronal magnetic field, *Astrophys. J., 318*, 428, 1987.

Horne, J. H., and S. L. Baliunas, A prescription for period analysis of unevenly sampled time series, *Astrophys. J., 302*, 757, 1986.

Hundhausen, A. J., An interplanetary view of coronal holes, in *Coronal Holes and High Speed Wind Streams*, edited by J. B. Zirker, pp. 225, Colorado Associated University Press, Boulder, CO, 1977.

Krieger, A. S., Temporal behavior of coronal holes, in *Coronal Holes and High Speed Wind Streams*, edited by J. Zirker, pp. 71, Colorado Assoc. Univ. Press, Boulder, CO, 1977.

Macdowall, R. J., M. D. Desch, M. L. Kaiser, R. G. Stone, R. A. Hess, A. Balogh, S. J. Bame, and B. E. Goldstein, The three-dimensional extent of a high speed solar wind stream, *Space Sci. Rev., 72*, 125, 1995.

Mursula, K., and B. Zieger, The 13.5-day periodicity in the Sun, solar wind, and geomagnetic activity: The last three solar cycles, *J. Geophys. Res., 101*, 27077, 1996.

Nolte, J. T., and E. C. Roelof, Large-scale structure of the interplanetary medium. I: High coronal source longitude of the quiet-time solar wind, *Solar Phys., 33*, 241, 1973.

Press, W. H., S. A. Teukolsky, W. T. Vetterling, and P. Flannery, *Numerical Recipes in FORTRAN of Scientific Computing,* pp. 569, Cambridge Press, New York, 1992.

Roelof, E. C., G. M. Simnett, R. B. Decker, L. J. Lanzerotti, C. G. Maclennan, T. P. Armstrong, and R. E. Gold, Reappearance of recurrent low-energy particle events at Ulysses/HI-SCALE in the northern hemisphere, *J. Geophys. Res., 102*, 11251, 1997.

Sargent, H. H. III., Recurrent geomagnetic activity: Evidence for long-lived stability in solar wind structures, *J. Geophys. Res., 90*, 1425, 1985.

Schou, J., et at., Helioseismic studies of differential rotation in the solar envelope by the solar oscillations investigation using the Michelson Doppler imager, *Astrophys. J., 505*, 390, 1998.

Smith, E. J., J. A. Slavin, and B. T. Thomas, The heliospheric current sheet: 3-dimensional structure and solar cycle changes, in *The Sun and Heliosphere in Three Dimensions*, edited by R. G. Marsden, pp. 267, D. Reidel, Dordrecht, 1986.

Snodgrass, H. B., Magnetic rotation of the solar photosphere, *Astrophys. J., 270*, 288, 1983.

Svalgaard, L., and J. M. Wilcox, Long term evolution of solar sector structure, *Solar Phys., 41*, 461, 1975.

Svalgaard, L., J. M. Wilcox, and P. H. Scherrer, The sun's magnetic sector structure, *Solar Phys., 45*, 83, 1975.

Trotter, D. E., and D. E. Billings, Longitudinal variations of a zone of solar activity, *Astrophys. J., 136*, 1140, 1962.

Vaughan, A. H., The magnetic activity of sunlike stars, *Science, 225*, 793, 1984.

Vaughan, A. H., S. L. Baliunas, F. Middelkoop, L. Hartmann, D. Mihalas, R. W. Noyes, and G. W. Preston, Stellar rotation in lower main sequence stars measured from time variations in H and K emission line fluxes: Initial results, *Astrophys. J., 250*, 276, 1981.

Table 1. Number of hourly averages of solar wind parameters used in analysis. Omni data were included through 11/30/98 (V) or 9/30/98 (B). Interplanetary spacecraft data were used only for the interval when the spacecraft were less than 3 AU from the Sun.

Source	Time interval	V only	V and B
Omni file	1963.9 - 1998.9	164,970	137,479
Mariner 2	1962.7 - 1962.9	1,429	0
Pioneer 6	1966.0 - 1967.7	3,258	3,258
Pioneer 7	1966.6 - 1967.8	2,841	2,841
Pioneer 10	1972.3 - 1972.9	4,041	3,919
Pioneer 11	1973.3 - 1974.0	5,028	4,145
Helios 1	1974.9 - 1981.0	42,458	24,329
Helios 2	1976.0 - 1980.2	26,472	14,015
Voyager 1	1977.7 - 1978.3	2,949	2,943
Voyager 2	1977.6 - 1978.4	4,137	4,120
Pioneer Venus Orb.	1978.9 - 1992.8	73,103	45,717
Ulysses	1990.0 - 1991.4	4,077	4,068
Total		334,763	246,834

Table 2. Definition of solar cycles used to average the solar wind data and the number of hourly values in each interval.

Cycle	Years included	Sign of B_r	# of V points	# of B_r points
A	1962.1 to 1966.74	As measured	14,066	6,877
B	1966.74 to 1977.54	Reversed	107,481	78,618
C	1977.54 to 1988.34	As measured	159,721	122,012
D	1988.38 to 1998.75	Reversed	60,296	39,327

Table 3. Statistics of the OMNI data set used in the time-series analysis

	V	B_r
Number of hours covered	306,897	305,386
Number of hourly averages	164,791 (53.7%)	169,962 (55.7%)
12-hour averages in Cycle A	989	618
12-hour averages in Cycle B	5785	6226
12-hour averages in Cycle C	5651	5746
12-hour averages in Cycle D	4066	3972
Total	16,491 (64.4%)	16,562 (65.1%)

Table 4. Selected measurements of solar rotation periods.

Measurement	Year	Synodic Period, days	Reference
Solar wind speed and radial IMF	1962-1998	27.03±0.02	This work
Solar wind speed	1964-1975	27.02	[*Gosling et al.*, 1977]
Magnetic sector boundary crossings	1924-1974	27.0 & ~28.5	[*Svalgaard and Wilcox*, 1975]
Equatorial coronal holes	1972-1973	~27.1	[*Krieger*, 1977]
Coronal magnetic field	1976-1986		[*Hoeksema and Scherrer*, 1987]
Northern hemisphere		26.9	
Southern hemisphere		28.1	
Photospheric magnetic field at equator	?	26.91	[*Snodgrass*, 1983]
Photospheric equatorial dipole	?	27.0	[*Hoeksema and Scherrer*, 1987]
Solar envelope	1996		[*Schou et al.*, 1998]
0.995 R_s	(144 days)	27.32±0.02	
0.95 R_s		26.5	

Figure Captions

Figure 1. Time-averaged variations of solar wind speed versus solar longitude for ten assumed values of the solar rotation period (given on the right). The tic marks on the left and right scales for each trace represent a speed of 450 km/s. The error bars indicate probable errors calculated from the spread of values in each longitude column in the time-longitude matrix described in the text.

Figure 2. The difference between the highest and the lowest speeds for the time-averaged speed-versus-longitude curves as a function of solar rotation period from 25 to 31 days.

Figure 3. Monthly-averaged sunspot numbers for the past 40 years. The start and stop times of our Cycles A-D, when the sign of B_r is reversed, are shown at the top.

Figure 4. The difference between the highest and the lowest values of $B_r(-1)^N$ for the time-averaged $B_r(-1)^N$-versus-longitude curves as a function of solar rotation period from 25 to 31 days.

Figure 5. Time-averaged profiles of V and $B_r(-1)^N$ versus longitude for a solar rotation period of 27.03 days, given separately for Cycles A-D. The horizontal lines in the right-hand panel indicate $B_r(-1)^N = 0$ nT.

Figure 6. The same as Figures 2 and 4, but given separately for Cycles A-D. The dashed line indicates a period of 27.03 days.

Figure 7. Lomb-Scargle periodograms calculated from 12-hour averages of hourly averages of V and $B_r(-1)^N$ in the OMNI data base.

Figure 8. The same as Figure 7 with an expanded time scale for periods of 26 to 29 days. The lower curves, without data points, are the periodograms calculated for a random distribution of each parameter sample at the same times as the data in the OMNI file.

Figure 9. A periodogram of B_r calculated from 12-hour averages of Pioneer Venus Orbiter (PVO) data and comparison with the periodogram calculated from the OMNI data base for Cycle C. The actual period observed at Venus has been shifted to the equivalent synodic period at Earth according to Equation 9. The vertical dashed line indicates a period of 27.03 days.

Figure 10. Periodograms $B_r(-1)^N$ calculated separately for periods of sunspot maximum and minimum and rising and declining activity, as defined in the text.

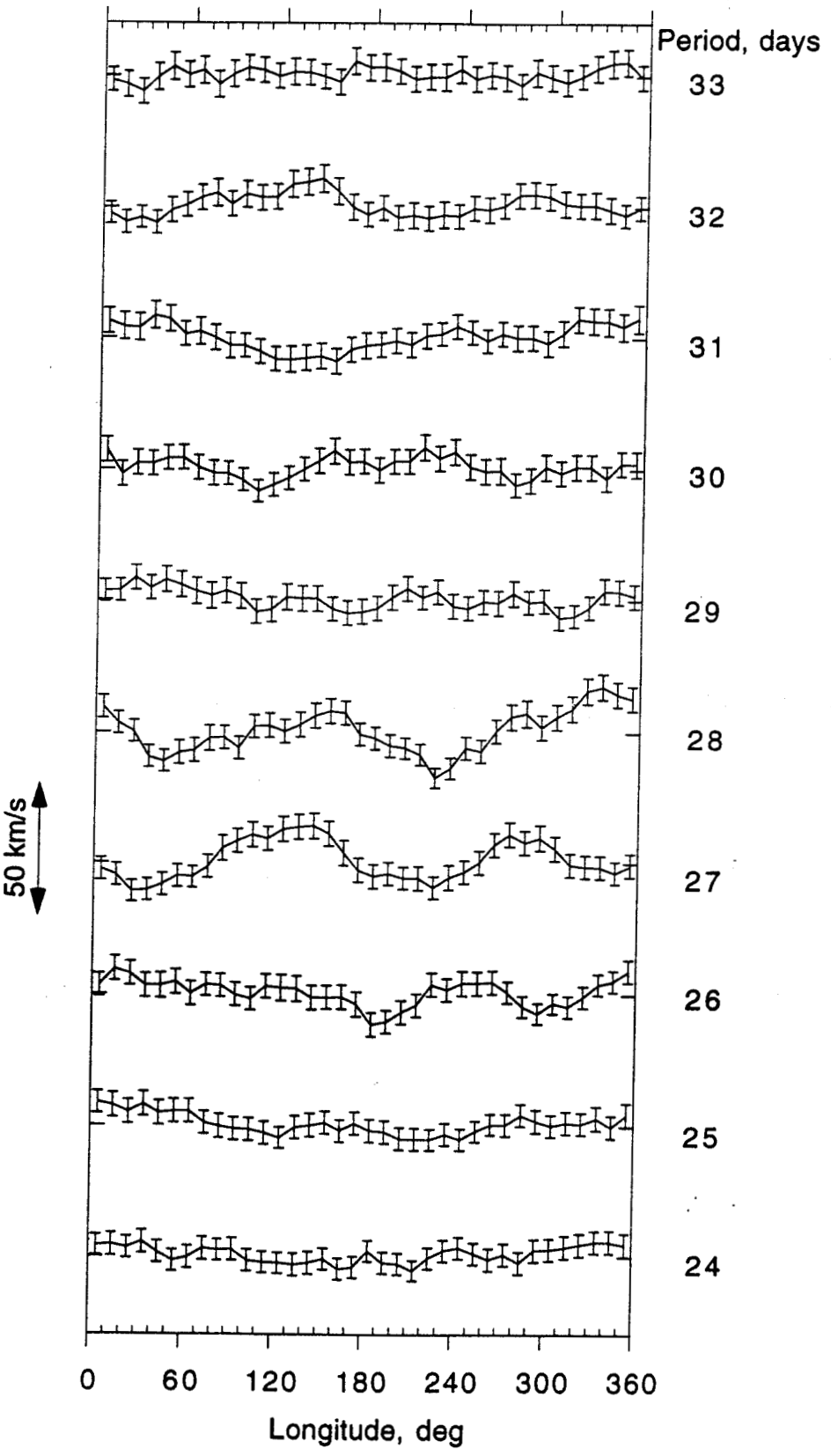
Period, days
33
32
31
30
29
28
27
26
25
24
50 km/s
0
60
120
180
240
300
360
Longitude, deg

Fig 1

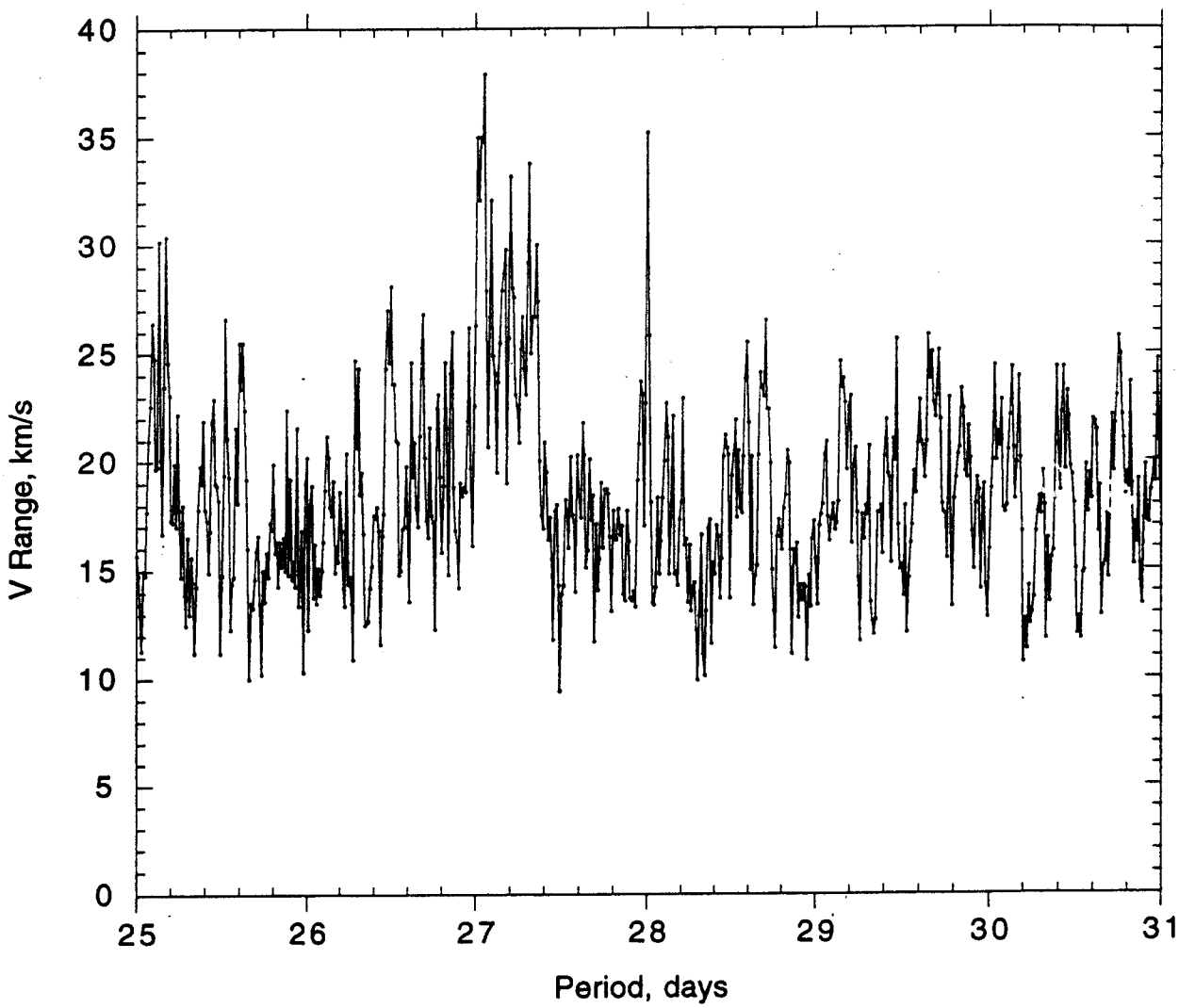

Fig 2

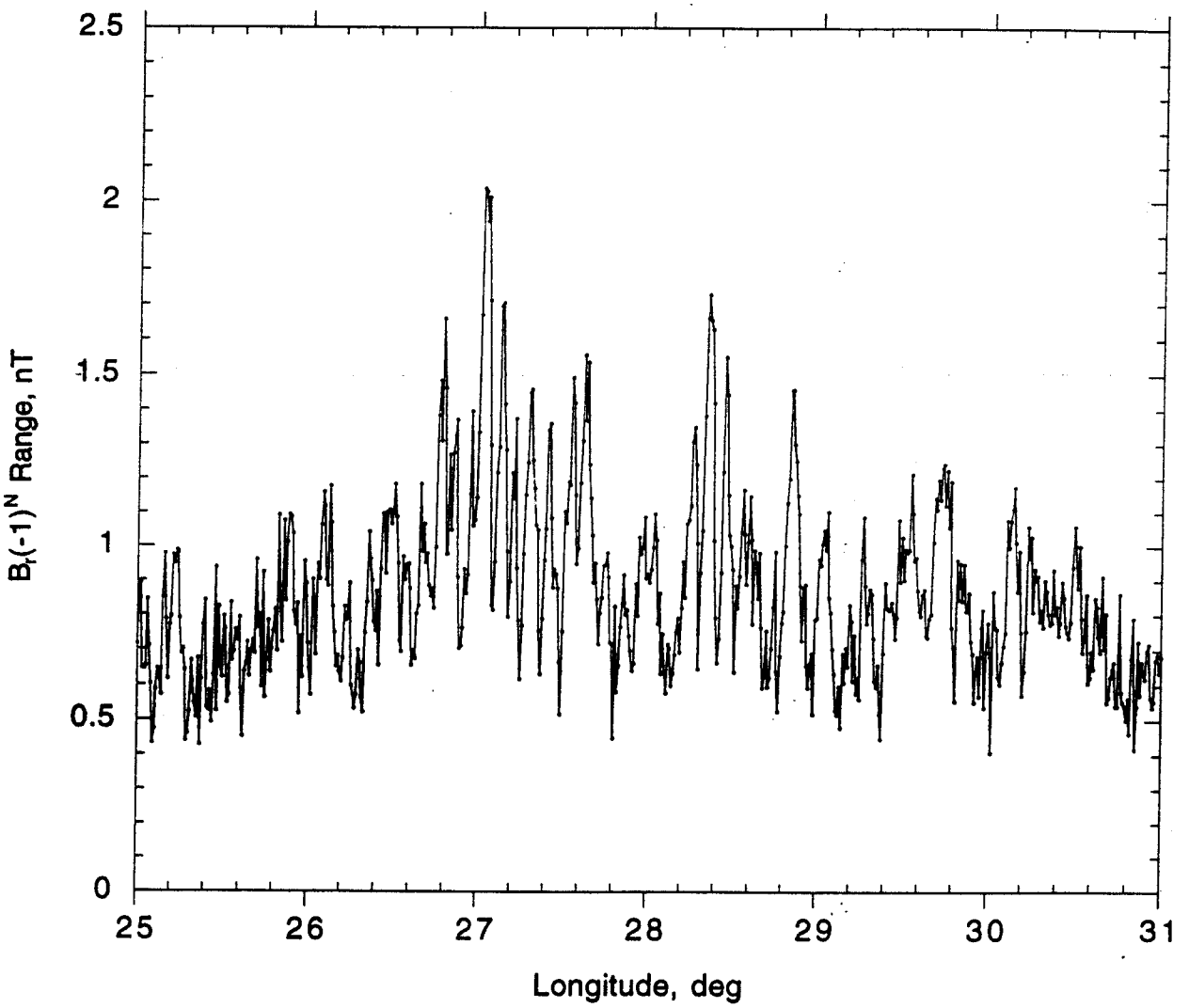

Fig 4

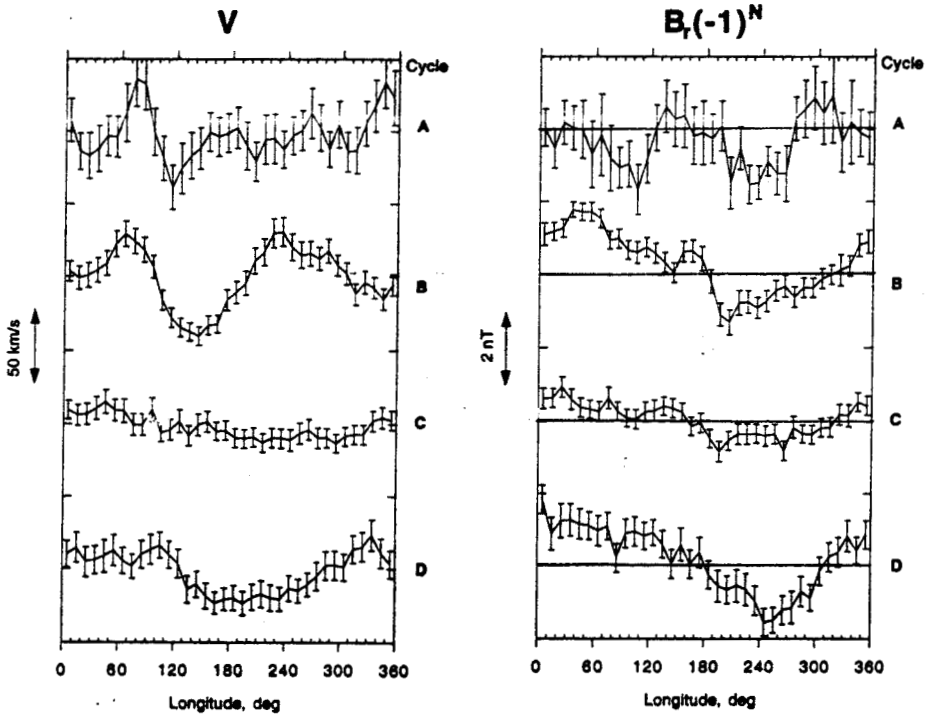
V
$B_r(-1)^N$
Cycle
A
B
C
D
50 km/s
2 nT
0
60
120
180
240
300
360
Longitude, deg

Fig 5

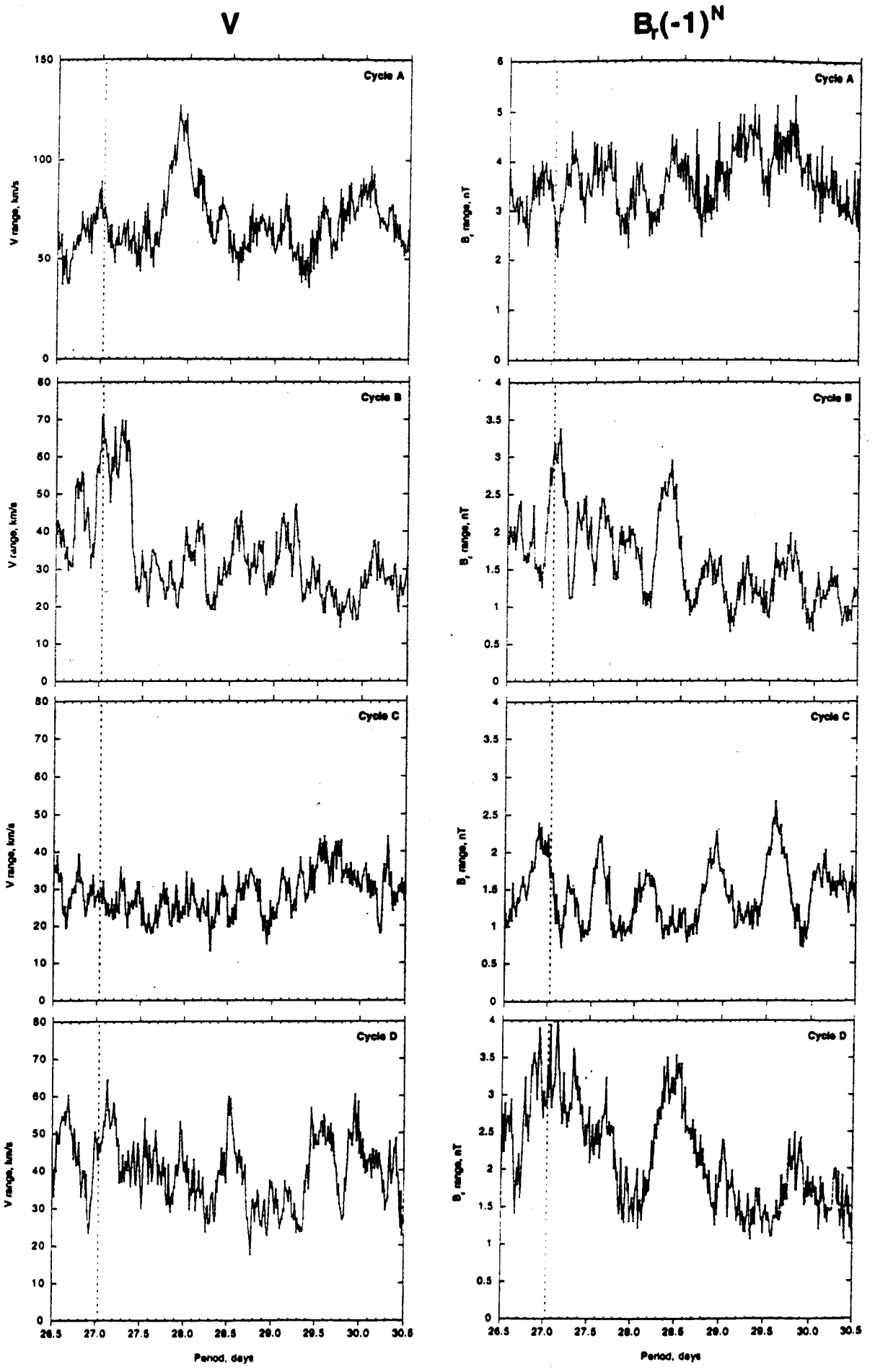
V
$B_r(-1)^N$
Cycle A
Cycle B
Cycle C
Cycle D
V range, km/s
B_r range, nT
Period, days

Fig 6

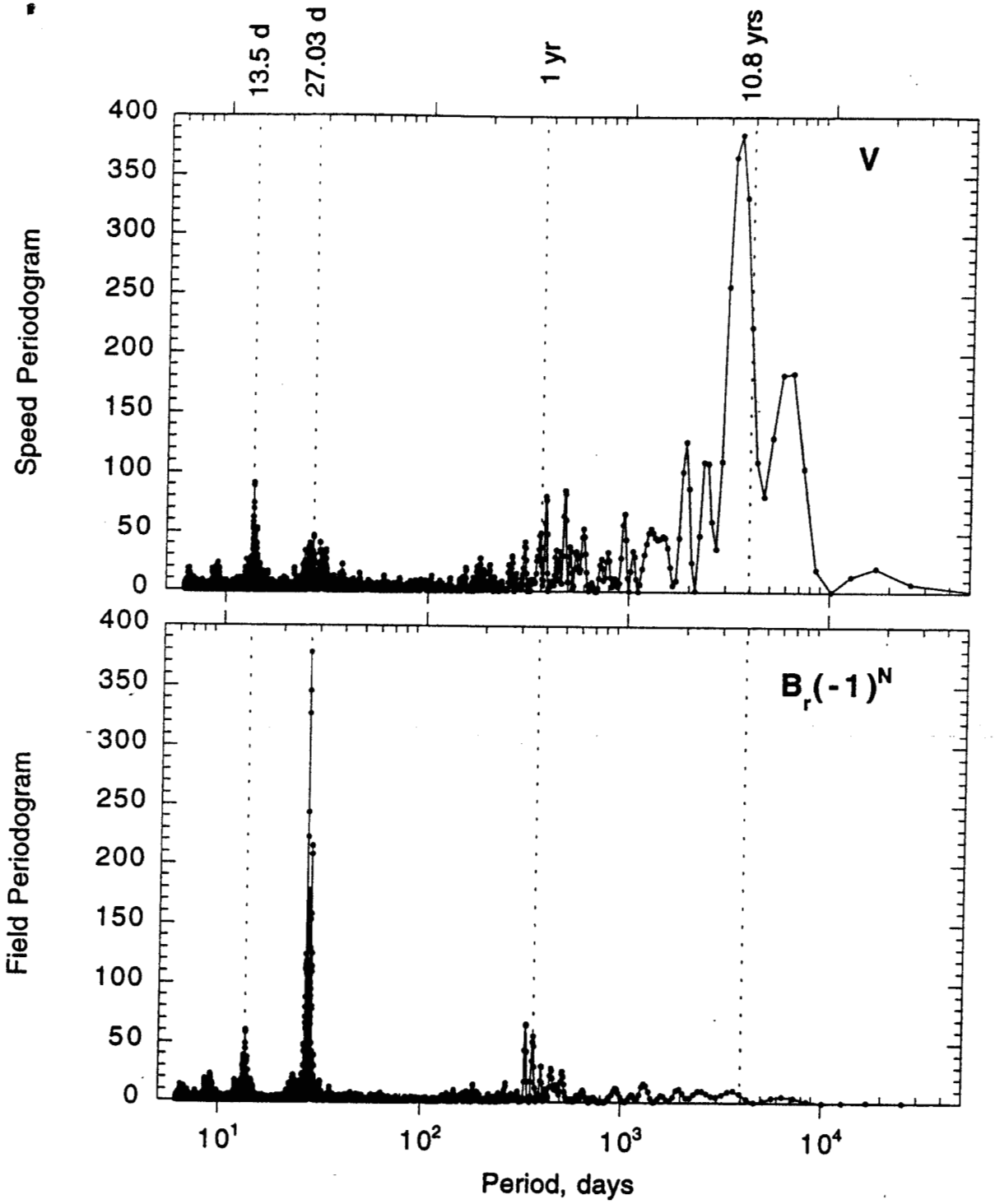
13.5 d
27.03 d
1 yr
10.8 yrs
Speed Periodogram
V
Field Periodogram
$B_r(-1)^N$
Period, days

Fig 7

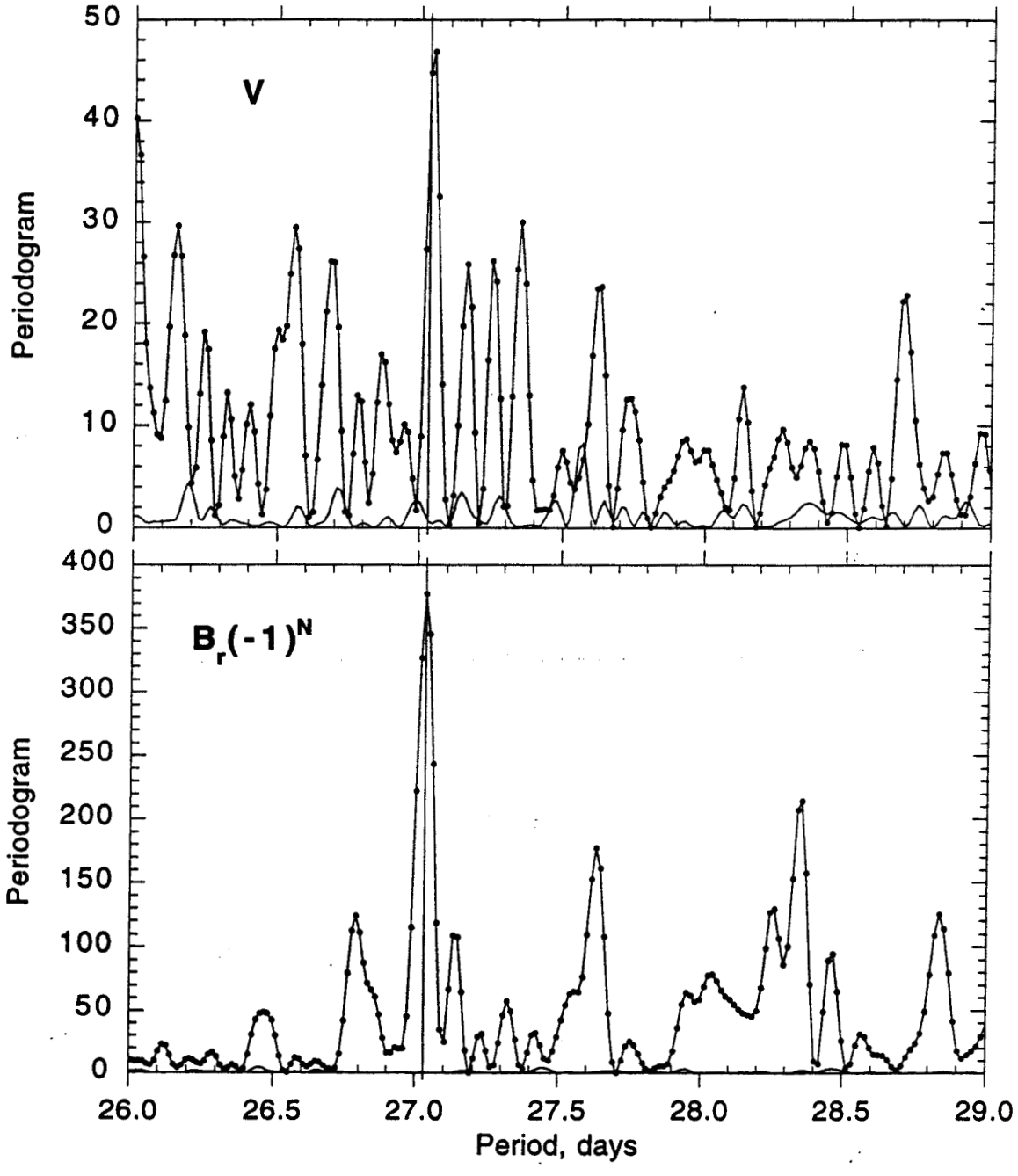
V
$B_r(-1)^N$
Periodogram
Periodogram
Period, days
0
10
20
30
40
50
0
50
100
150
200
250
300
350
400
26.0
26.5
27.0
27.5
28.0
28.5
29.0

Fig 8

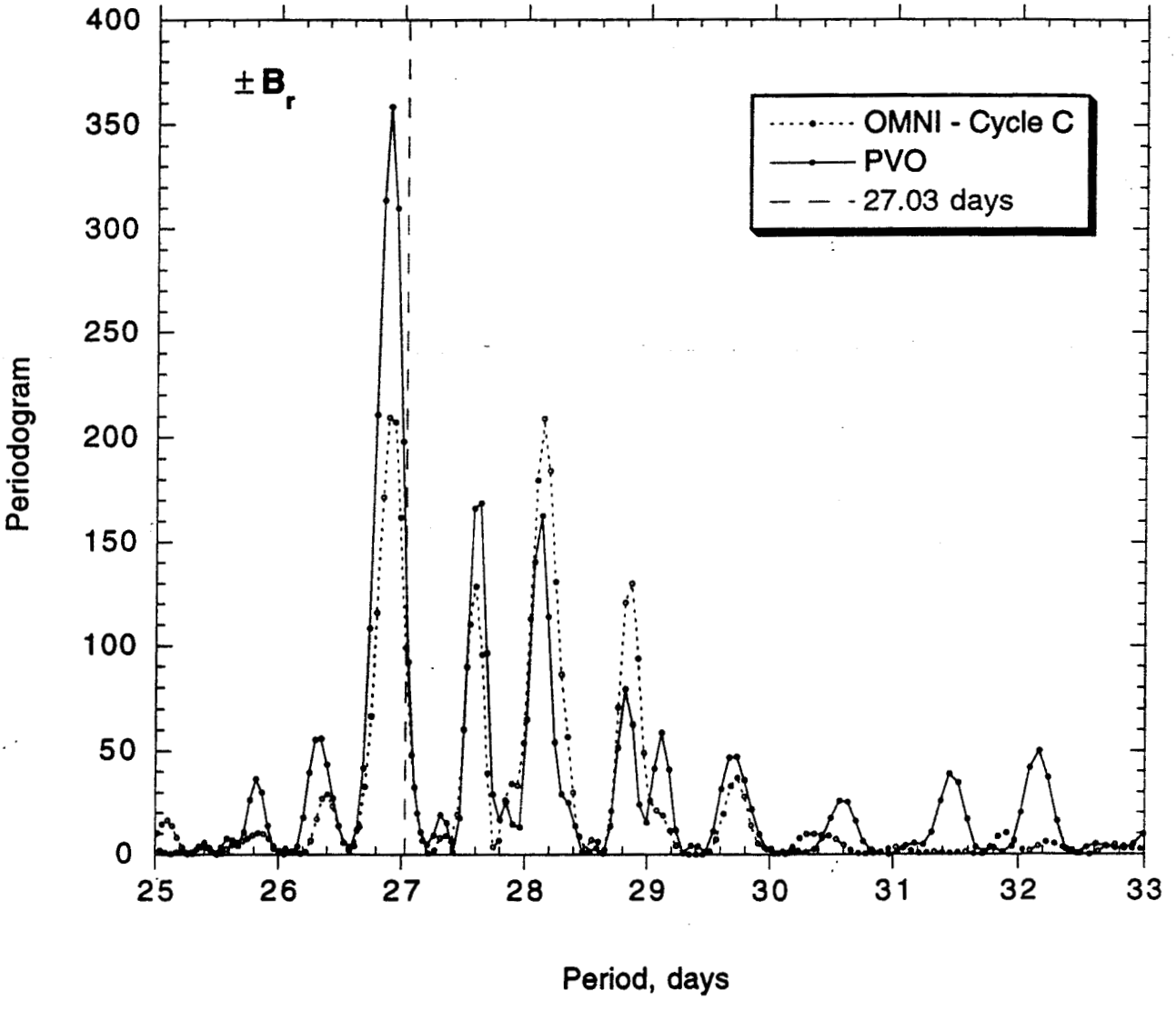
±B_r
OMNI - Cycle C
PVO
27.03 days
Periodogram
Period, days
400
350
300
250
200
150
100
50
0
25
26
27
28
29
30
31
32
33

Fig 9

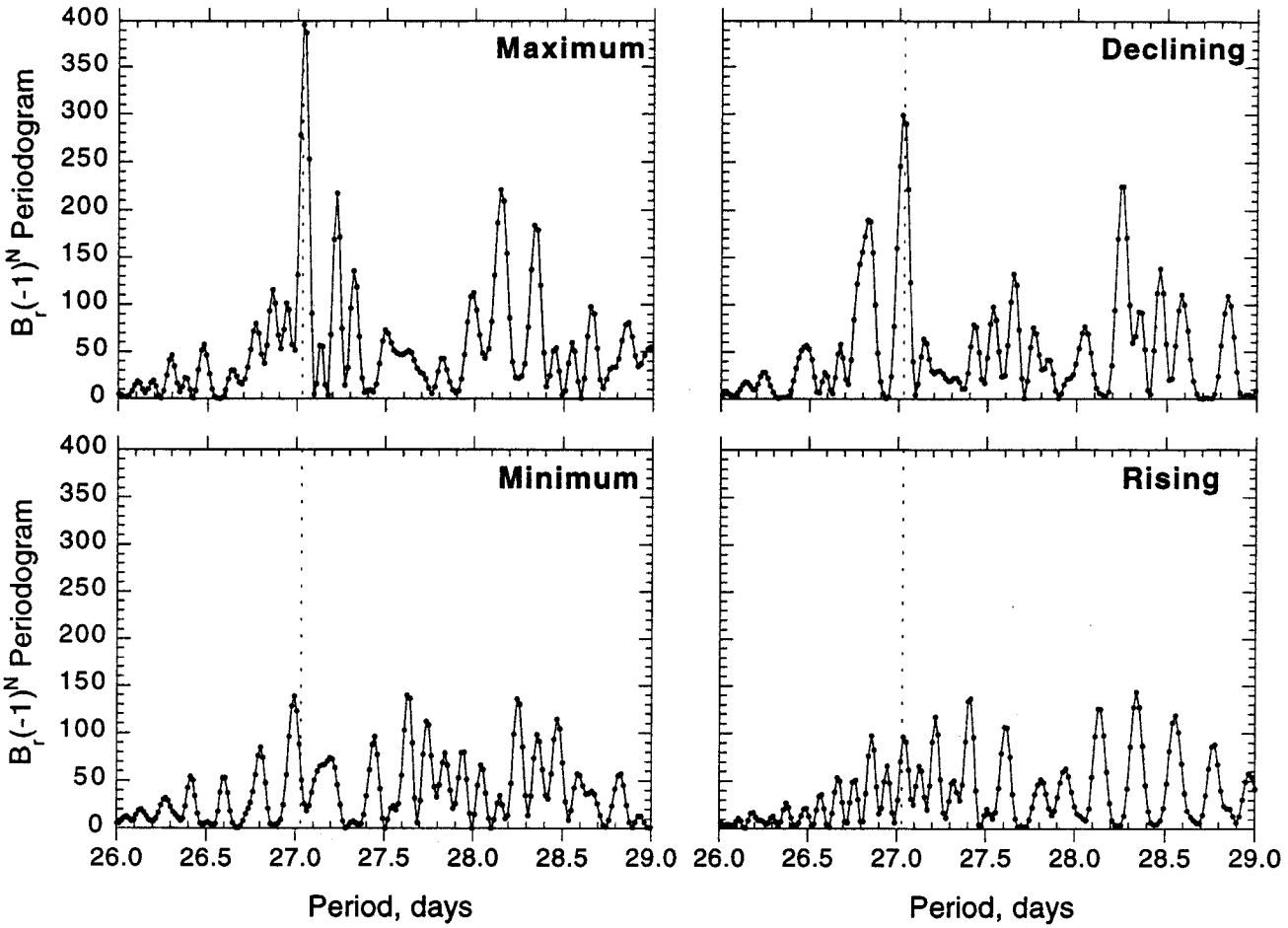
Maximum
Declining
Minimum
Rising
$B_r(-1)^N$ Periodogram
$B_r(-1)^N$ Periodogram
0
50
100
150
200
250
300
350
400
26.0
26.5
27.0
27.5
28.0
28.5
29.0
Period, days
Period, days

Fig 10